Colorimetric assay for the detection of dopamine using bismuth ferrite oxide (Bi2Fe4O9) nanoparticles as an efficient peroxidase-mimic nanozyme

Mehri Razavi, Alexandre Barras, Madjid Ifires, Abir Swaidan, Maryam Khoshkam, Sabine Szunerits, Mohsen Kompany-Zareh, Rabah Boukherroub

Colorimetric assay for the detection of dopamine using bismuth ferrite oxide ($Bi_2Fe_4O_9$) nanoparticles as an efficient peroxidase-mimic nanozyme

Mehri Razavi[a,b], Alexandre Barras[b], Majdid Ifires[b,c], Abir Swaidan[b], Maryam Khoshkam[d], Sabine Szunerits[b], Mohsen Kompany-Zareh[a,e], Rabah Boukherroub[b*]

[a]*Department of Chemistry, Institute for Advanced Studies in Basic Sciences, 45137-66731, Zanjan, Iran*

[b]*Univ. Lille, CNRS, Centrale Lille, Univ. Polytechnique Hauts-de-France, UMR 8520 - IEMN, F-59000 Lille, France*

[c]*Research Center of Semi-conductor Technology for Energy, CRTSE - 02, Bd. Dr. Frantz FANON, B.P. 140 Algiers-7, Merveilles 16038, Algeria*

[d]*Department of Chemistry, Faculty of Science, Mohaghegh Ardabili University, 56199-11367, Ardabil, Iran*

[e]*Department of Chemistry, Dalhousie University, 6274 Coburg Road, P.O. Box 15000, Halifax NS B3H 4R2, Canada*

*Corresponding author: Rabah Boukherroub
Univ. Lille, CNRS, Centrale Lille, Univ. Polytechnique Hauts-de-France, UMR 8520 - IEMN, F-59000 Lille, France
Tel: +33362531724; Fax: +33362531701
E-mail: rabah.boukherroub@univ-lille.fr

Graphical Abstract

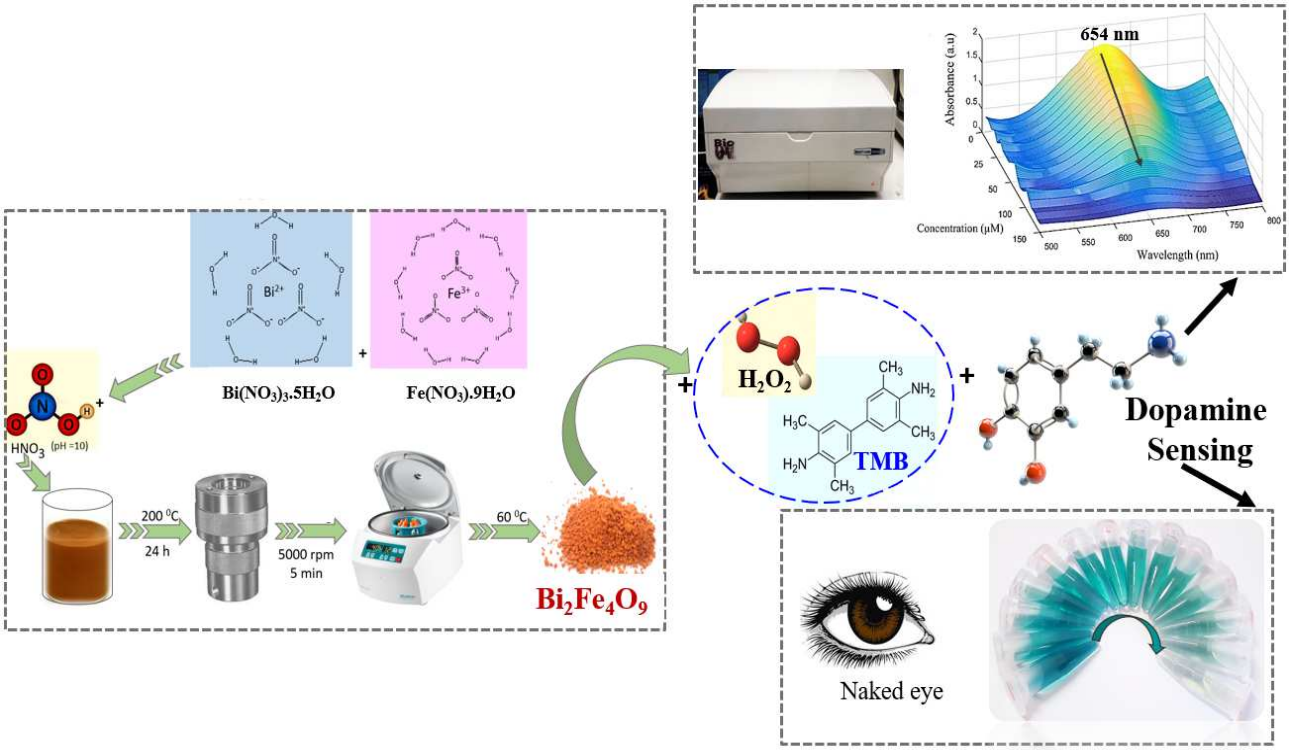

Highlights

- $Bi_2Fe_4O_9$ nanozyme as a simple and low-cost colorimetric sensor was developed for easy dopamine detection
- The sensor achieved good performance with a linear range from 0.15 to 50 μM and a detection limit of 51 nM
- The nanozyme was reused up to 4 cycles without a significant decrease in its performance

Abstract

This work describes the preparation of ternary bismuth ferrite oxide nanoparticles ($Bi_2Fe_4O_9$ NPs) with an enzyme mimetic activity for dopamine (DA) qualitative and quantitative detection. $Bi_2Fe_4O_9$ NPs were prepared using a facile, low cost, and one-pot hydrothermal treatment. The chemical composition, morphology, and optical properties of $Bi_2Fe_4O_9$ nanozyme were characterized using different techniques such as Fourier-transform infrared spectra (FTIR), X-ray diffraction pattern (XRD), X-ray photoelectron spectroscopy (XPS), thermo-gravimetric analysis (TGA), dynamic light scattering (DLS), field-emission scanning electron microscopy (FESEM) imaging, FESEM-energy dispersive X-ray spectroscopy (EDS), UV-vis absorption, and fluorescence emission spectroscopy. $Bi_2Fe_4O_9$ NPs were utilized to catalyze the oxidation of a typical chromogenic peroxidase substrate, 3,3',5,5'-tetramethylbenzidine (TMB), to form the blue-colored oxidized product (oxTMB), in the presence of hydrogen peroxide (H_2O_2). All reactions occurred in acetate buffer solution (pH 3.5) to generate hydroxyl radicals ($^{\bullet}OH$) and the kinetics were followed by UV-vis absorbance at 654 nm. The steady-state kinetic parameters were obtained from the Michaelis-Menten equation and exhibited a good catalytic efficiency of $Bi_2Fe_4O_9$ NPs as enzyme mimetics. Michaelis–Menten constant (K_m) values were estimated as 0.07 and 0.73 mM for TMB and H_2O_2, respectively. The presented method is efficient, rapid, cost-effective, and sensitive for the colorimetric detection of dopamine with a linear range (LR) from 0.15 to 50 μM and a detection limit (LOD) of 51 nM. The proposed colorimetric sensor was successfully applied for the detection of different concentrations of dopamine in spiked fetal bovine serum (FBS) and horse serum (HS) samples. It is anticipated that $Bi_2Fe_4O_9$ nanozyme holds great potential in biomedical analysis and diagnostic applications of dopamine-related diseases.

Keywords: $Bi_2Fe_4O_9$ nanozyme, 3,3',5,5'-tetramethylbenzidine (TMB), Peroxidase-like activity, Dopamine, Colorimetric assay.

1. Introduction

Dopamine (DA), 4-(2-aminoethyl) benzene-1,2-diol), is a biogenic monoamine and one of the quite important catecholamine neurotransmitters (NT), which plays significant key roles in the mammalian central nervous such as memory, learning, cognition, emotions, renal, hormonal, and cardiovascular systems [1-3]. The abnormal level of dopamine concentration in the human body can lead to serious neurological syndromes and various diseases like Alzheimer, Parkinson, Huntington, senile dementia, and Schizophrenia [4-7].

Therefore, the measurement of the dopamine level in biological fluids with high accuracy and sensitivity is an extremely important factor for early diagnosis of diseases and development of therapeutic approaches [3, 8]. Various analytical strategies have been developed to detect the DA level, including high-performance liquid chromatography (HPLC) [9], capillary electrophoresis (CE) [10, 11], field-effect transistor (FET)-based biosensor [12], fluorometry [13, 14], random lasers (RL) with incoherent feedback [15], electrochemiluminescence (ECL) [16], and electrochemical methods [17, 18]. However, all these methods have several constraints; they often require complex and advanced pre-treatment processes, long analysis times, high-costs, sophisticated instruments, and trained personnel [4, 8]. In this regard, many studies have been focused on elucidating the colorimetric assays for dopamine identification, because of their intrinsic advantages of simple assay design, time-saving, high efficiency, and most importantly, easy visual detection [3, 4, 7].

Traditionally, natural enzymes as biological catalysts have been applied in colorimetric analysis systems. A common example is the horseradish peroxidase enzyme (HRP). To keep up with the more efficient performance of natural enzymes, they must be applied under relatively mild conditions. Natural enzymes feature high substrate-specificity and efficiency. However, they are limited by some inherent drawbacks such as the high-cost of preparation and purification, easy denaturation, the extreme sensitivity of catalytic activity towards environmental changes such as pH or temperature, difficulties in recovery, limited storage, and availability [19, 20]. As a potential alternative, an emerging group of nanomaterials has recently been considered. The choice of enzyme-mimics based on nanomaterials rather than natural enzymes has well-confirmed the rational decision to detect dopamine and conquer these limitations. The significant properties of nanozymes include a high surface-to-volume ratio, low-cost, simple preparation, tunable activity, high stability, long-term storage, and

easy preparation. As evidenced by the mentioned advantages, nanozymes have been exploited to further evaluate their analytical performance in bio-nanotechnology [21-23].

Yan and colleagues were the first to point out Fe_3O_4 NPs as an enzyme-mimic for TMB substrate [24]. In recent years, ferrite-based enzyme-like nanomaterials have generated tremendous attention [25-27], because of their potential for various applications such as gas sensors [28], catalyst for ammonia oxidation [29], photocatalysts for hydrophobic and organic pollutants degradation [26, 30], removal of heavy metal ions [31], memory devices [32], data storage [33], and spintronic devices [34]. Lu and colleagues successfully synthesized and applied $CuFe_2O_4/Cu_9S_8$/polypyrrole (PPy) ternary nanotubes as a suitable colorimetric platform for easy detection of dopamine and H_2O_2 molecules [35]. Chen et al. reported that Fe/NC-800 exhibited an enhanced catalytic activity for dopamine sensing [36]. Liu and co-workers reported that $ZnO/ZnFe_2O_4$/graphene foam (ZZFO/GF) is an excellent colorimetric-catalyst to distinguish hydroquinone (HQ) molecules with the assistance of H_2O_2 molecule [37]. Su and co-workers demonstrated the use of the spinel $ZnFe_2O_4$ NP-decorated ZnO nanofiber as an effective colorimetric platform with a peroxidase-like activity for glucose detection in urine samples [38]. Hou et al. fabricated $Fe_3O_4@C@MnO_2$ composite as a triple-enzyme mimetic activity to catalyze TMB oxidation reaction and was successfully applied for dopamine detection [39].

In this investigation, we report, for the first time, the application of irregular sheet-like $Bi_2Fe_4O_9$ nanoparticles as one of the Fe-based nanozymes for the colorimetric detection of nanomolar concentration of dopamine in aqueous media. Fe active sites (Fe^{2+}/Fe^{3+}) and the d-orbitals of Fe^{3+} in $Bi_2Fe_4O_9$ NPs operate in a Fenton-like reaction to improve the catalytic oxidization of 3,3',5,5'-tetramethylbenzidine (TMB), a chromogenic substrate, in presence of H_2O_2 in acetic acid medium (pH=3.5) to yield a deep-blue product (oxTMB). The simultaneous existence of large irregular-sheets and Fe, as a transition-metal ion, located at FeO_6 (octahedral) and FeO_4 (tetrahedral) in the unit cell of $Bi_2Fe_4O_9$ nanozyme, were useful factors to reduce H_2O_2 to $^{\bullet}OH$ radical and increase the oxidation of TMB molecules. In presence of dopamine (DA), as efficient $^{\bullet}OH$ radical scavenger, the colorimetric signal of the $Bi_2Fe_4O_9/H_2O_2$/TMB/DA was significantly lower than that of $Bi_2Fe_4O_9/H_2O_2$/TMB system, and the deep-blue color of the ox-TMB was changed to fade-blue color. On the basis of this quenching behavior, the catalytic activity of $Bi_2Fe_4O_9$ nanozyme was exploited to design a selective and sensitive colorimetric sensor for dopamine concentration determination in fetal bovine serum (FBS) and horse serum (HS) samples. The results of the study showed that

$Bi_2Fe_4O_9$ NPs could be developed as a promising group of nanozyme materials for dopamine diagnostic purposes and biomedical applications.

2. Experimental

2.1. Synthesis of $Bi_2Fe_4O_9$ nanoparticles

As shown in **Scheme S1**, $Bi_2Fe_4O_9$ NPs were prepared using the hydrothermal method, according to a previous procedure with a slight modification [27]. First, $Bi(NO_3)_3{\cdot}5H_2O$ (4.85 g) and $Fe(NO_3)_3{\cdot}9H_2O$ (4.04 g) powders were dissolved in 13 mL of deionized water (DIW) and 2 mL of nitric acid (HNO_3 65%) at room temperature (RT) to form solution A. Throughout the process, the above solution was kept under vigorous magnetic stirring for 30 min. Then, 75 mL of potassium hydroxide (KOH, 8 M) as a mineralizer was slowly dropped into solution A to adjust the pH to 8-9 with rapid stirring. It is worth noticing that a red-brown suspension of a bismuth-ferrite was formed at room temperature. In hydrothermal processing, the uniform suspension was transferred into a Teflon-lined autoclave and heated at 200 ^oC for 24 h. Then, the autoclave was cooled to room temperature and the formed precipitate was collected by centrifugation at 5,000 rpm for 5 min and washed at least three times with deionized water and ethanol (95%) to remove residual ions. Furthermore, the produced $Bi_2Fe_4O_9$ powder was dried in an oven at 60 ^oC overnight for later use. Ultimately, the produced $Bi_2Fe_4O_9$ NPs were yellow-orange color at room temperature.

2.2. Peroxidase-like activity of $Bi_2Fe_4O_9$ nanoparticles

In a typical assay, different concentrations of $Bi_2Fe_4O_9$ (0-30 µg/mL) were added to 225 µL of TMB (0.3 mM dissolved in ethanol), 225 µL of H_2O_2 (5 mM) in acetate buffer (pH 3.5, 0.1 M) and the final volume of solution was adjusted to 1.5 mL. The mixture was incubated for 25 min at 45 ^oC. All chemical reagents were exactly prepared before every experiment. UV-vis spectrometry (500 to 800 nm) was used to investigate the absorbance variation at 654 nm due to oxidation of TMB substrate.

2.3. Steady-state kinetics for the determination K_m and V_{max}

The catalytic efficiency and the rate of enzyme reactions of $Bi_2Fe_4O_9$ NPs can be determined by the Michaelis–Menten equation. To assess the kinetics parameters, the utilization of different substrate concentrations (TMB or H_2O_2) is an essential factor. Under the optimized conditions, kinetic experiments were determined by adding various concentrations of TMB chromogenic substrate (0.01-0.30 mM) at a fixed concentration of

H_2O_2 (5 mM) in the first set of experiments. For the second set of kinetic experiments, the H_2O_2 concentration was varied from 0.1 to 5.0 mM while the concentration of TMB substrate was kept constant (0.3 mM). All experiments were carried out in the acetic acidic buffer (pH 3.5, 0.1 M) and the total volume of the mixture solutions was equal to 1.5 mL. UV-vis absorbance was recorded within the 500-800 nm range and the obtained V_{max}, and K_m values were compared with the kinetic parameters of other nanozymes.

2.4. Colorimetric assay for the detection of dopamine

To accurately investigate the efficacy of $Bi_2Fe_4O_9$ NPs (120 µL, 8 µg/mL) to detect dopamine, first, a solution of a fixed concentration of TMB (225 µL, 0.3 mM) and H_2O_2 (525 µL, 5 mM) in acetate buffer solution (pH=3.5, 0.1 M) was prepared. Afterward, various dopamine concentrations (0-150 µM) were added to the above solution; the total volume was 1.5 mL. The entire reaction mixture was quickly shacked then incubated at 45 °C for 25 min. The course of the reaction was monitored using UV-vis spectrometer (500-800 nm). At the end of incubation, UV-vis absorbance values were recorded at 654 nm and the obtained maximum absorbance was used to generate the calibration curve and also to determine the limit of detection of dopamine.

2.5. Selectivity and reproducibility of $Bi_2Fe_4O_9$ nanoparticles

To evaluate the selectivity of the designed colorimetric assay, various amino acids and small molecules such as alanine (Ala), cysteine (Cys), arginine (Arg), lysine (Lys), glutathione (GSH), uric acid (UA), ascorbic acid (AA), lactose (Lac), glucose (Glu), fructose (Fru), and different ions (K^+, Na^+, Mg^{2+}, and Ca^{2+}) were separately added to the mixture solution of TMB (0.3 mM), H_2O_2 (5 mM), and $Bi_2Fe_4O_9$ NPs (8 µg/mL) in acetate buffer (pH 3.5, 0.1 M). The concentration of applied interfering components was two times the concentration of dopamine (100 µM). All the above solutions were incubated for 25 min at 45 °C, and their UV-vis spectra were measured in the 500-800 nm range. The characteristic reproducibility of the synthesized $Bi_2Fe_4O_9$ nanozyme was examined for four catalytic cycles of TMB oxidation under the optimized experimental conditions ($Bi_2Fe_4O_9$ (8 µg/mL), TMB (0.3 mM), H_2O_2 (5 mM), acetate buffer (pH 3.5, 0.1 M), T=45 °C, and incubation time=25 min).

2.6. Procedure for dopamine detection in real samples

For dopamine analysis in real samples, 1µL of pure fetal bovine serum (FBS) and horse serum (HS) samples were diluted in phosphate buffer saline (PBS pH 7.4) and then $Bi_2Fe_4O_9$ nanozyme (8 µg/mL), H_2O_2 (5 mM), and TMB (0.3 mM) were added. The total volume of the solution was maintained at 1.5 mL using acetate buffer (pH 3.5, 0.1 M). Afterward, different concentrations of dopamine (1, 5, and 10 µM) were introduced into the above mixture solution and incubated for 25 min at 45 ^oC. To detect the presence of dopamine in the FBS 1 (Sigma-Aldrich), FBS (Fisher Scientific), and HS (Fisher Scientific) samples, the corresponding changes in the absorbance spectra were monitored by UV-vis spectroscopy (500-800 nm). All experiments were performed in triplicates.

2.7. Detection of hydroxyl radicals (•OH) generation in the presence of $Bi_2Fe_4O_9$

In a typical assay, 0.2 mM of terephthalic acid (TA) was dissolved in ethanol. Eight mixtures were prepared as following: (**a**) H_2O_2 (5 mM) + $Bi_2Fe_4O_9$ NPs (8 µg/mL), (**b**) H_2O_2 (5 mM) + $Bi_2Fe_4O_9$ NPs (8 µg/mL) + dopamine (50 µM), (**c**) $Bi_2Fe_4O_9$ NPs (8 µg/mL), (**d**) $Bi_2Fe_4O_9$ NPs (8 µg/mL) + dopamine (50 µM), (**e**) H_2O_2 (5 mM), (**f**) H_2O_2 (5 mM) + dopamine (50 µM), (**g**) only TA (15 µl), and (**h**) TA (15 µl) + dopamine (50 µM) in acetate buffer (pH 3.5), and all solutions were incubated for 25 min at 45 °C. The total volume of eight tubes was filled to 1.5 mL. The change of fluorescence emission spectra (λ_{ex}=315 nm) was recorded in the 400–550 nm range by utilizing a Safas Xenius XC fluorescence spectrophotometer.

Moreover, to examine the presence of •OH radicals as one of the members of reactive oxygen species (ROS), *tert*-butyl alcohol (TBA) was used as a quencher. $Bi_2Fe_4O_9$ NPs (8 µg/mL), TMB (0.3 mM), H_2O_2 (5 mM), acetate buffer (pH 3.5, 0.1 M), TBA (0.5 mM) were incubated at 45 ^oC for 25 min (total volume of the solution was 1.5 mL). All absorption spectra of the solutions with or without TBA molecules were recorded at 564 nm.

3. Results and discussion

3.1. Characterization of $Bi_2Fe_4O_9$ nanoparticles

As observed in **Fig. 1**, the morphological and chemical composition of the as-prepared $Bi_2Fe_4O_9$ nanozyme were characterized by field emission scanning electron microscopy (FESEM) imaging and energy-dispersive X-ray (EDX) spectroscopy. The low and high magnification FESEM micrographs showed that $Bi_2Fe_4O_9$ consist of an irregular~~ly~~ sheet-like morphology (**Fig. 1A-C**).

The accumulation of initial bismuth and ferrite salts causes the random collision of Bi-Fe-O elements, which leads to an increase of the irregular sheet growth. The irregular particle shapes of $Bi_2Fe_4O_9$ were formed by considering the different growth rates in various directions. Taken together, the results of elemental distribution mapping and EDX analysis (**Fig. 1D**) clearly illustrate the presence of Bi, Fe, and O elements, which is in full agreement with the chemical composition of $Bi_2Fe_4O_9$ NPs. The atomic percentages of Bi, Fe, and O elements in the $Bi_2Fe_4O_9$ sample were equal to 15.77%, 21.15%, and 63.08%, respectively. It can be noticed that there is a deviation from the stoichiometric composition due to iron deficiency. As revealed in **Fig. 1E-G**, the elemental mapping of Bi (green), Fe (white), and O (red) has intelligibly confirmed the uniform distribution of mentioned elements on the surface of $Bi_2Fe_4O_9$ enzyme-mimicking nanomaterial [27, 31].

The hydrodynamic radius and particle size distributions of the synthesized $Bi_2Fe_4O_9$ NPs were measured by utilizing the dynamic light scattering (DLS) and zeta potential techniques, respectively (**Fig. 1H and I**). The average hydrodynamic diameter (d_{hydr}) of $Bi_2Fe_4O_9$ NPs was ~396 nm (3 measurements). In addition, the surface charge of $Bi_2Fe_4O_9$ was found to be -31.62 mV. Based on these results, $Bi_2Fe_4O_9$ NPs with a negative surface charge are expected to interact electrostatically with the positively charged chromogenic substrate (TMB) and efficiently catalyze the oxidation of TMB. The positive surface charge of TMB was brought by the presence of two amine groups [40-42].

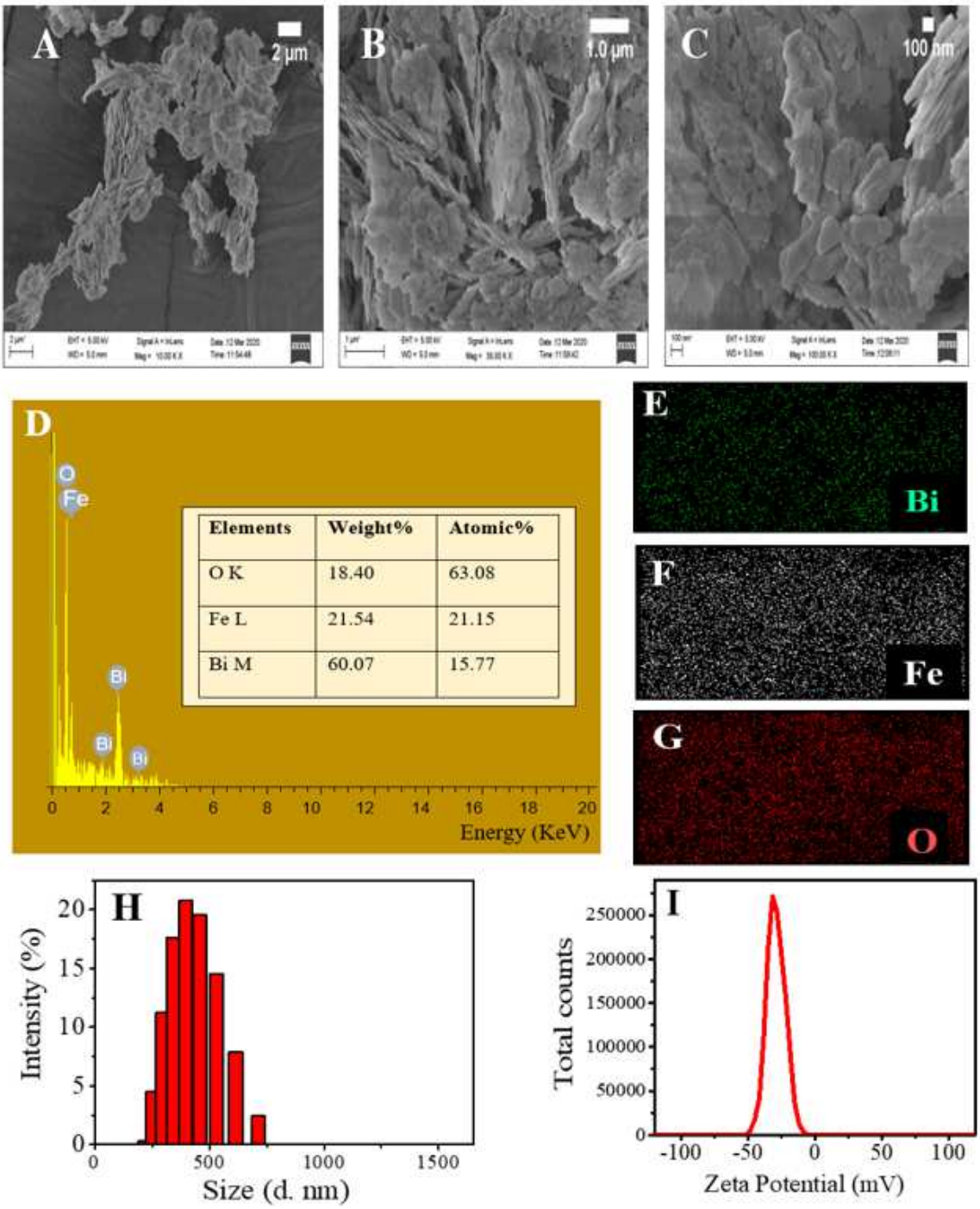

Fig. 1. FESEM images at low and high magnifications (**A-C**), EDX spectrum (**D**), elemental mappings for Bi (**E**), Fe (**F**), and O (**G**), DLS size distribution (**H**), and zeta potential (**I**) of the as-prepared $Bi_2Fe_4O_9$ NPs.

Fig. S1 depicts the FTIR spectrum of the $Bi_2Fe_4O_9$ NPs (700-4000 cm^{-1}), which indicates the presence of diverse functional groups on the surface of the NPs. The spectrum comprises broad and weak absorption bands at 3441 and 1636 cm^{-1} related to hydroxyl groups stretching and bending vibrations from water molecules or intermolecular hydrogen bonds,

respectively. The strong absorption peak at 1384 cm^{-1} belongs to the residual NO_3^- group incorporated during the preparation of $Bi_2Fe_4O_9$ sample. Besides, bismuth ferrite is an isostructural compound and contains tetrahedral FeO_4, octahedral FeO_6, and octahedral BiO_6 units. The vibration band at 808 cm^{-1} is assigned to Fe-O stretching vibrations of FeO_4 and FeO_6, and also Bi-O in the BiO_6 octahedral pairs [31, 43, 44].

The results of the thermogravimetric analysis (TGA) and derivative thermogravimetric (DTG) of $Bi_2Fe_4O_9$ NPs in the 30–980 °C temperature range are shown in **Fig. S2**. TGA analysis of $Bi_2Fe_4O_9$ NPs demonstrates four clear steps of weight loss: (I) 50 °C, (II) 150 °C, (III) 220 °C, (IV) 657 °C corresponding to the mass reduction of 0.79%, 0.79%, 0.47% and 5.49%, respectively. The first step belongs to water and residual organic solvent evaporation, and the second step of the significant mass loss was probably due to the decomposition of the ternary metal oxide structure of BFO [45]. By increasing the temperature (978.5 °C), the TGA curve of $Bi_2Fe_4O_9$ features an approximate loss of 8.21% of its total mass and 91.79% of the residual mass was left at the end of heating.

X-ray photoelectron spectrometry (XPS) was utilized to examine the elemental composition and the oxidation states of the as-prepared $Bi_2Fe_4O_9$ NPs (**Fig. 2A-D**). The XPS survey spectrum of $Bi_2Fe_4O_9$ NPs revealed the presence of Bi 4f, Bi 4d, Bi 4p, C 1s, Fe 2p, and O 1s peaks (**Fig. 2A**). In the survey spectrum of $Bi_2Fe_4O_9$ NPs (**Fig. 2A**), the narrow peak of C 1s observed at 285 eV is most likely due to surface contamination. On the basis of the XPS results, the atomic percentages of Bi, Fe, and O elements in $Bi_2Fe_4O_9$ NPs were 13.72, 17.62, and 68.66 at.%, respectively. The results reflect Fe deficiency, in accordance with EDX analysis, even though there was no evidence for the existence of another crystalline phase (see XRD analysis below).

The O 1s wide scan spectrum (**Fig. 2B**) can be fitted with four Gaussian curves at around 528.8 eV (O1), 530.3 eV (O2), 531.4 eV (O3), and 532.9 eV (O4), which are respectively ascribed to lattice M–O–M bonds, surface lattice oxygen, the presence of oxygen vacancies, and absorbed H_2O or surface carbonate [27, 46, 47]. As shown in **Fig. 2C**, the wide scan of Fe 2p XPS profile can be fitted with two components at binding energies of 710.1 and 723.6 eV, that are respectively assigned to Fe $2p_{3/2}$ and Fe $2p_{1/2}$. These binding energies data confirmed the occurrence of two oxidation states (+2 and +3) in the BFO oxide. The high-resolution spectrum of Fe $2p_{3/2}$ can be deconvoluted into two Gaussian peaks at 711.4 and 725.4 eV which belong to the Fe^{3+} valence state in the $Bi_2Fe_4O_9$. The two peaks at 709.4 and 723.1 eV can be attributed to Fe $2p_{1/2}$ that correlate with the existence of Fe^{2+} ions in Fe-O bands. Furthermore, the two satellite peaks located at 717.9 eV (Sat. I) and 732.2 eV (Sat. II)

both belong to Fe^{3+} species in the $Bi_2Fe_4O_9$ NPs [27, 47-49]. The Bi 4f XPS plot (**Fig. 2D**) can be deconvoluted into two distinct peaks ascribed to Bi $4f_{7/2}$ peak at 158.2 eV and Bi $4f_{5/2}$ peak at 164.1 eV. The spin-orbit splitting of Bi 4f (5.90 eV) corresponds to bismuth ion in the +3-valence state in the synthesized $Bi_2Fe_4O_9$ NPs [26, 27, 50].

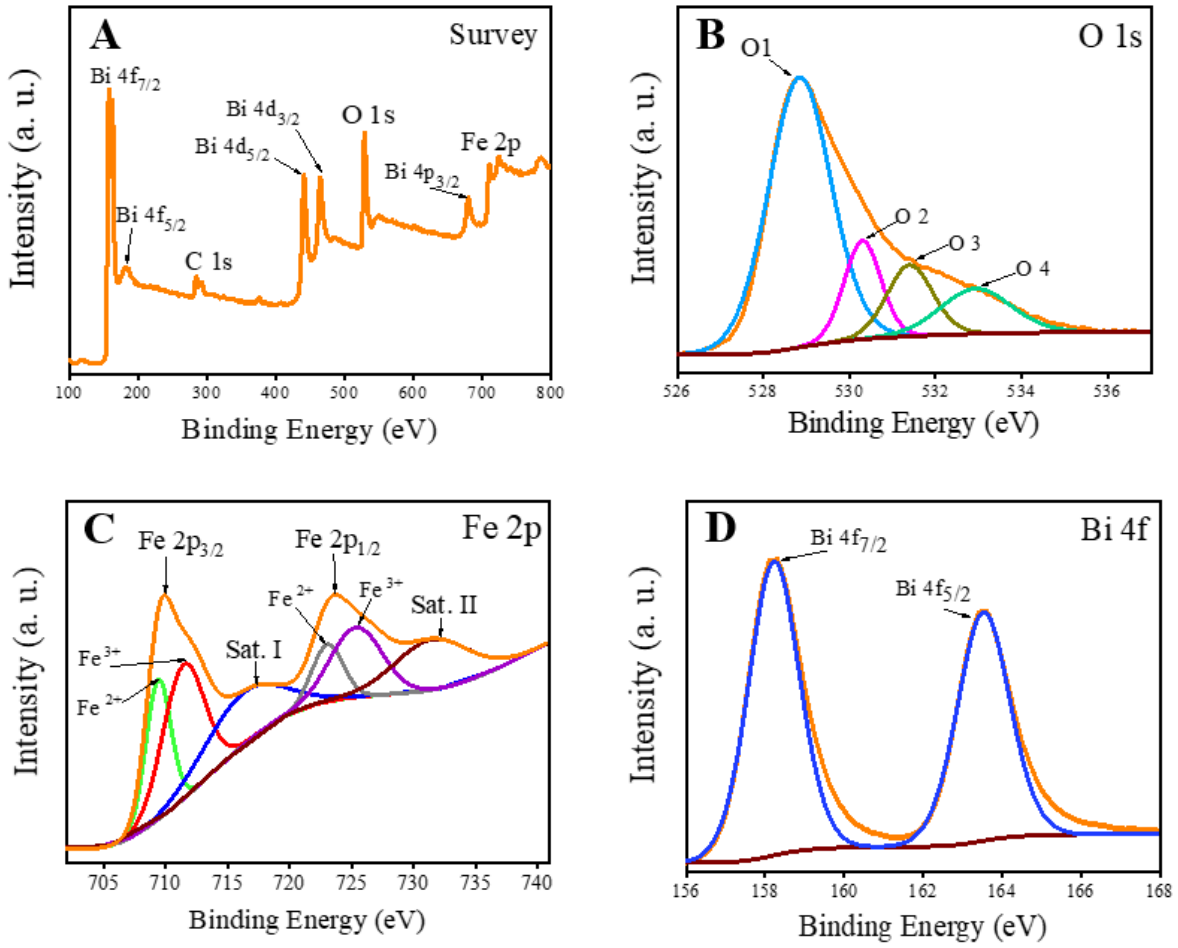

Fig. 2. (**A**) XPS survey spectrum, and high-resolution XPS spectra of (**B**) O 1s, (**C**) Fe 2p, and (**D**) Bi 4f regions of $Bi_2Fe_4O_9$ NPs.

The phase purity and crystallinity of the as-prepared $Bi_2Fe_4O_9$ NPs were analyzed by X-ray diffraction (XRD) patterns (**Fig. S3**). The characteristic diffraction peaks located at 2θ angles of 14.78°, 20.88°, 22.40°, 23.88°, 24.90°, 25.72°, 26.88°, 28.06°, 28.94°, 29.72°, 30.80°, 33.58°, 35.52°, 36.62°, 37.54°, 39.20°, 44.18°, 45.40°, 46.82°, 48.82°, 49.50°, 50.68°, 52.04°, 54.36°, 55.30°, 56.54°, 58.8°, 61.56, 64.68°, and 67.22° can be perfectly indexed to the orthorhombic $Bi_2Fe_4O_9$ structure with (001), (020), (200), (120), (210), (021), (201), (121), (211), (002), (220), (130), (310), (022), (202), (212), (140), (132), (141), (240), (411), (420), (123), (142), (402), (332), (431), (004), (342), and (530), respectively ((JCPDS File No. 00-025-0090). The crystalline planes with d-spacing values related to the above crystal

planes of $Bi_2Fe_4O_9$ sample were determined to be 5.99, 4.25, 3.97, 3.72, 3.57, 3.46, 3.32, 3.18, 3.09, 3.00, 2.90, 2.67, 2.52, 2.45, 2.39, 2.30, 2.05, 2.00, 1.93, 1.86, 1.83, 1.80, 1.75, 1.68, 1.65, 1.63, 1.57, 1.51, 1.44, and 1.39 Å, respectively. The sharp diffraction peaks in the XRD pattern obviously indicate that $Bi_2Fe_4O_9$ has a well-crystallized structure without the existence of other impurities [44, 51-53]

3.2. Peroxidase-like activity of $Bi_2Fe_4O_9$ nanoparticles

In this catalytic process, the enzyme-mimetic activity of $Bi_2Fe_4O_9$ NPs was examined for the oxidation of TMB, as electron-donor species, to ox-TMB in the presence of H_2O_2 as electron-acceptor species. The decomposition of H_2O_2 molecules was catalyzed by Fe species on the surface of $Bi_2Fe_4O_9$ nanozyme. Ferrite ions in $Bi_2Fe_4O_9$ nanozyme are located at FeO_6 octahedral and FeO_4 tetrahedral in the unit cell. Fe is a useful transition metal ion in Fenton reactions to reduce H_2O_2 to $^{\bullet}OH$ radicals. Different oxidation forms of Fe cations like Fe^{3+}/Fe^{2+} and the d-orbitals of Fe^{3+} were consecutively produced and used in the suggested Fenton-reaction cycle. Besides the Fe active-sites, the large irregular sheet area of $Bi_2Fe_4O_9$ created more reactive sites and enhanced the peroxidase-like activity of $Bi_2Fe_4O_9$ nanozyme. To mimic the Fenton-like reaction, Fe ions and the produced $^{\bullet}OH$ radicals played a key role in oxidizing TMB molecules to the blue-coloured form of TMB semiquinone dimer [43, 44, 47, 54-58].

TMB oxidation in presence of $Bi_2Fe_4O_9$ nanozyme is believed to occur through a Fenton-like reaction, as summarized in **Eq. 1-4** (**Scheme 1**). In a weakly acidic medium, $Bi_2Fe_4O_9$ nanozyme successfully decomposes H_2O_2 molecules to hydroxyl radical ($^{\bullet}OH$), as an effective intermediate molecule (**Eq. 3**) to carry out the oxidation of TMB molecules in H_2O_2/TMB/$Bi_2Fe_4O_9$ system (**Eq. 4**) at room temperature. The oxidized TMB substrate can be visualized by monitoring the maximum absorbance peak at 654 nm.

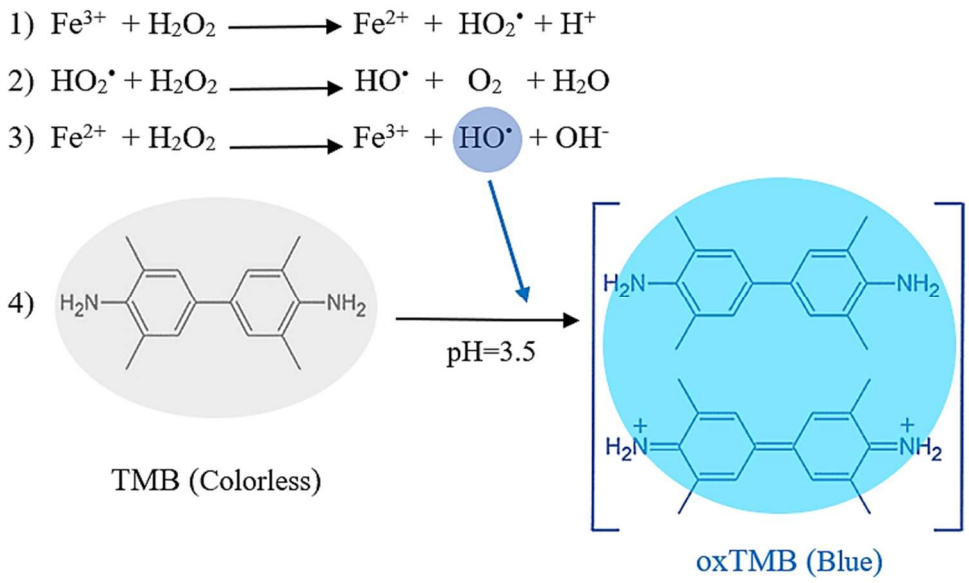

Scheme 1. Schematic illustration of the plausible mechanism of TMB oxidation by H_2O_2 in the presence of $Bi_2Fe_4O_9$ NPs.

Under the reaction conditions, the meaningful effect of the absence and presence of $Bi_2Fe_4O_9$ nanozyme catalyst and H_2O_2 molecule on the catalytic oxidation of TMB substrate was investigated and the variation of UV–vis spectra are displayed in **Fig. 3(i-iii)**. Insert in **Fig. 3** indicated the recorded photographs of the oxTMB color-change system. The experimental systems consisting of only H_2O_2 or $Bi_2Fe_4O_9$ had no obvious effect on the oxidation reaction of TMB and the absorbance signal of the solutions was close to the background (**Fig. 3i**). Meanwhile, the addition of $Bi_2Fe_4O_9$ to TMB only slightly increased the TMB oxidation (**Fig. 3ii**). After the introduction of both $Bi_2Fe_4O_9$ and H_2O_2 solutions into the fresh TMB reagent, the peroxidase-like activity $Bi_2Fe_4O_9$ improved and considerably decomposed H_2O_2 molecules to $^{\bullet}OH$ as active intermediates for oxidation of TMB (**Fig. 3iii**). In an acidic medium (pH 3.5), the occurrence of the oxidation reaction was confirmed by the naked eyes through the color change from the colorless mixtures of H_2O_2/TMB and Bi_2Fe4O_9/TMB to the deep-blue color of H_2O_2/TMB/$Bi_2Fe_4O_9$, and also the produced ox-TMB recorded a remarkable absorbance at around 654 nm (**Fig. 3**). All of the results demonstrated that the presence of both $Bi_2Fe_4O_9$, as intrinsic peroxidase-like activity catalyst, and H_2O_2, as inherent oxidant, was responsible for the remarkable increase of the oxidation rate of TMB substrate.

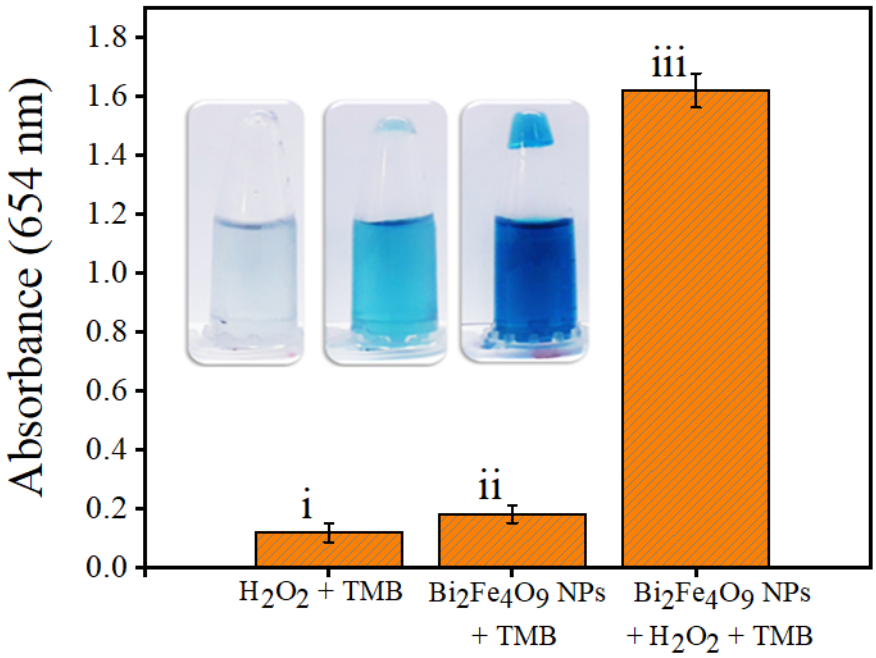

366

367 **Fig. 3.** Relative UV–vis absorption spectra changes of different solutions containing acetate
368 buffer (pH 3.5, 0.1 M) and reaction components recorded after 25 min incubation at T=45 °C.
369 Typical photographs of the oxidized TMB (oxTMB) [from left to right: (**i**) H_2O_2+TMB
370 without $Bi_2Fe_4O_9$ NPs (colorless), (**ii**) TMB+$Bi_2Fe_4O_9$ without H_2O_2 (slightly blue), and (**iii**)
371 TMB+ H_2O_2+$Bi_2Fe_4O_9$ NPs (blue)]. Reaction condition: $Bi_2Fe_4O_9$ NPs (8 µg/mL), TMB (0.3
372 mM), H_2O_2 (5 mM), T=45 °C (For each solution, n=3).

373 *3.3. Experimental condition optimization*

374 In order to have a better insight into the reaction performance, the enzyme-like catalytic
375 reaction was performed under different experimental conditions by varying TMB, H_2O_2, and
376 $Bi_2Fe_4O_9$ concentrations, pH, temperature, and the incubation time of the reaction [24, 59].
377 The effects of the different concentrations of $Bi_2Fe_4O_9$ NPs (1-30 µg/mL), TMB (0-0.7 mM),
378 and H_2O_2 (0-8 mM), pH (pH=1-12), incubation time (5-50 min), and temperature (15-60 °C)
379 was investigated and clearly depicted in **Fig. S4A-F**. Optimizing the concentrations of
380 $Bi_2Fe_4O_9$, TMB, and H_2O_2 molecules were manifested by the maximum value of absorbance
381 at 654 nm. As depicted in **Fig. S4A-C**, the optimum absorbance was recorded using 8 µg/mL,
382 0.3 mM, and 5 mM of $Bi_2Fe_4O_9$, TMB, and H_2O_2 respectively. In this study, the optimum
383 concentrations were utilized to carry out the following experiments. The result in **Fig. S4D**
384 demonstrated that pH values higher than 3.5 may cause the decomposition of H_2O_2 substrate
385 into H_2O and O_2 molecules. Consequently, the rate of the formation of $^{\bullet}OH$ radicals was
386 decreased, and the distinct blue color-change was obtained only in an acidic condition.
387 Therefore, the pH value of 3.5 was selected as the optimum pH that illustrated the blue-dark

color solution with the highest absorbance at 654 nm. Another effective factor was the reaction temperature. In each case, the influence of the temperature on the peroxidase activity of mimic-catalyst was investigated in a slightly acidic buffer (pH 3.5, 0.1 M). The catalytic activity of the $Bi_2Fe_4O_9$ sharply increased when the temperature was raised from 10 to 45 °C, and then decreased at temperatures higher than 45 °C. Therefore, the subsequent experiments were performed at the optimal temperature of 45 °C (**Fig. S4E**). Moreover, incubation time plays an important role in the decomposition of H_2O_2 and the accomplishment of the oxidation reaction for which the selected optimal-time corresponds to 25 min (**Fig. S4F**). As expected, the mimic-catalytic activity of $Bi_2Fe_4O_9$ depends on the concentration, pH, temperature, and reaction-time, similar to other nanozymes reported in the literature. According to the optimized values, it can be expected that $Bi_2Fe_4O_9$ nanozyme as a metal oxide-type mimic catalyst can be applied for sensitive and accurate detection of dopamine.

3.4. Kinetic study of $Bi_2Fe_4O_9$ NPs and the determination of Michaelis-Menten constants

To explore the steady-state kinetic of $Bi_2Fe_4O_9$ as a peroxidase mimic nanozyme, various concentrations of H_2O_2 and TMB as two different substrates were used to determine the initial rate of H_2O_2 and TMB in acetate buffer (pH 3.5, 0.1 M) at 45 ^oC. In order to accurately calculate the initial velocity rate, the Beer-Lambert Law was applied (**Eq. 5**).

$$V = \frac{\Delta c}{\Delta t} = \frac{\frac{\Delta A}{\varepsilon b}}{\Delta t} \quad (5)$$

where A, b, ε, t and V represent respectively the absorbance at 654 nm, the optical path length (1 cm), the molar absorptivity coefficient of oxTMB (39000 $M^{-1}.cm^{-1}$), the time (min), and the reaction rate. In the time span of 0-30 min, **Fig S5 (A, B)** depicts the relationship between the recorded UV-vis absorption spectra at 654 nm with the constant concentration of one substrate (TMB or H_2O_2) and varying the concentration of the other substrate in the reaction mixture. UV-vis absorption was dramatically increased and then reached a steady-state level for both TMB (under the constant concentration of H_2O_2) and H_2O_2 (under the constant concentration of TMB) substrates. And at this investigation time, the Michaelis-Menten kinetic model fitted well the variation of the absorption process.

To determine the kinetic parameters, the Michaelis-Menten model is one of the earliest descriptions and the best-known models to comprehensively investigate the value of nanozyme kinetics activity. Michaelis-Menten kinetics of $Bi_2Fe_4O_9$ peroxidase-mimic

catalyst was determined by keeping constant the concentration of TMB or H_2O_2 as a targeted substrate and varying the concentration of the other molecule in a time-scan mode, simultaneously. Kinetic parameters (K_m and V_{max}) were calculated using the Lineweaver–Burk plots of the double reciprocal of the Michaelis-Menten **Eq. 6**:

$$\frac{1}{\nu} = \frac{1}{[S]} \times \frac{K_m}{V_{max}} + \frac{1}{V_{max}} \quad (6)$$

where [S], ν, V_{max}, and K_m refer to the substrate concentration, the initial reaction rate, the maximum reaction rate, and Michaelis-Menten constant, respectively [6, 22, 60]. The steady-state kinetic measurements were conducted for both TMB and H_2O_2 as enzyme substrates (**Fig. 4A-B**). Under the optimized conditions, the Michaelis-Menten curves were generated for TMB, at different concentrations of TMB (0.01-0.30 mM) and a fixed concentration of H_2O_2 (5 mM), **Fig. 4A**, and also for H_2O_2 at various concentrations of H_2O_2 (0.1-5 mM) and a constant concentration of TMB (0.30 mM), **Fig. 4B**. According to the obtained results, the Michaelis-Menten constant (K_m) and maximum reaction rate (V_{max}) for H_2O_2/TMB/$Bi_2Fe_4O_9$ system were calculated and drawn via fitting the data into the Lineweaver Burk double reciprocal plots (**Fig. 4A** and **B** insets).

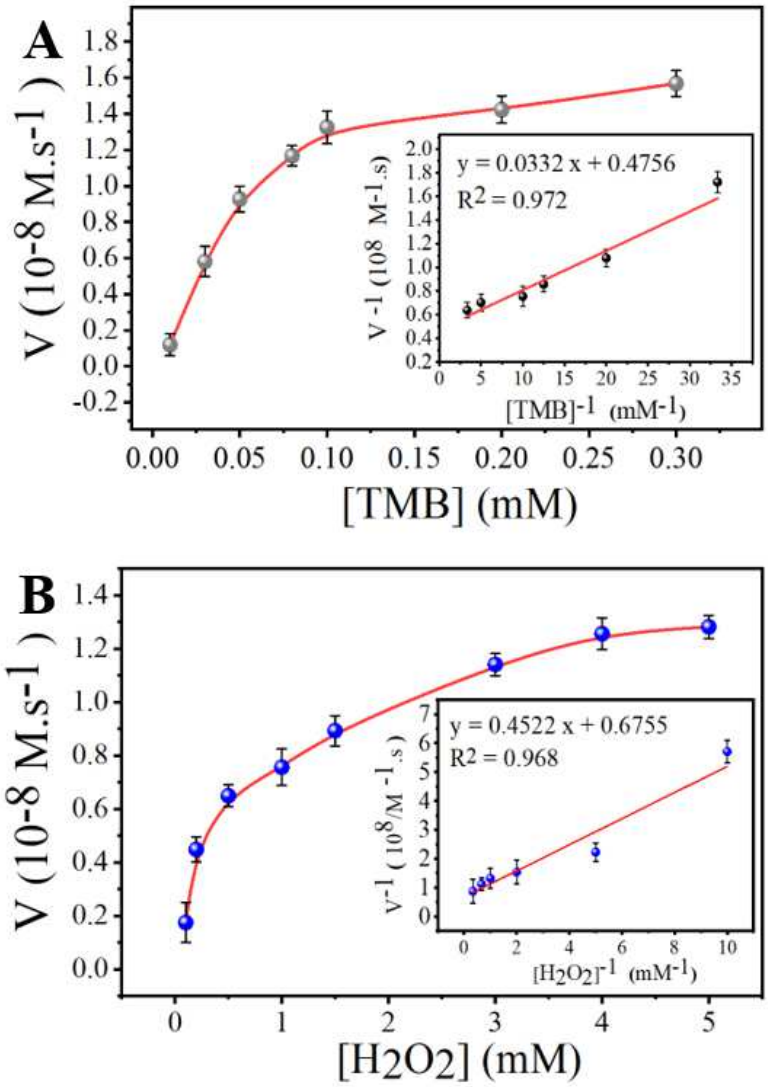

435

436 **Fig. 4.** Steady-state kinetic experiments of $Bi_2Fe_4O_9$ NPs at (**A**) different concentrations of
437 TMB (0.01-0.30 mM) and fixed concentration of H_2O_2 (5 mM) substrates, and (**B**) varying
438 concentrations of H_2O_2 (0.1-5 mM) and constant concentration of TMB (0.3 mM) substrates.
439 Insets: the linear calibration curves for the determination of TMB and H_2O_2. Reaction
440 conditions: $Bi_2Fe_4O_9$ NPs (8 µg/mL), acetate buffer (pH 3.5, 0.1 M), T=45 °C, and incubation
441 time=25 min. UV-vis measurements were repeated three times.

442

443 **Table 1** summarizes the obtained enzyme kinetic parameters (K_m and V_{max}) in
444 comparison to the horseradish peroxidase (HRP) enzyme and other nanomaterials reported in
445 the literature. For TMB and H_2O_2 substrates in H_2O_2/TMB/$Bi_2Fe_4O_9$ system, the obtained
446 constant K_m and V_{max} parameters equaled to 0.07 and 0.73 mM, and 2.17 and 1.56 ($\times 10^{-8}$)
447 $M.s^{-1}$, respectively. In this context, the Michaelis-Menten constant (K_m) is an effective
448 parameter to emphasize the affinity between the $Bi_2Fe_4O_9$ as an enzyme-like catalytic with

peroxidase substrate (TMB or H_2O_2). The lower value of K_m of $Bi_2Fe_4O_9$ in comparison to natural HRP and other nanozyme catalysts refer to its stronger affinity towards both TMB and H_2O_2 substrates. Besides, the lower K_m value of $Bi_2Fe_4O_9$ NPs for H_2O_2 means that the higher catalytic response of $Bi_2Fe_4O_9$ NPs was obtained using a small concentration of H_2O_2 substrate. This means that the decomposition of H_2O_2 into $^{\bullet}OH$ radical can be accelerated to oxidase TMB molecules. According to the obtained K_m and V_{max} constants, $Bi_2Fe_4O_9$ features a good affinity towards TMB and H_2O_2 for peroxidase-mimic activity.

Table 1

Comparison of the steady-state kinetic parameters (Michaelis-Menten constant (K_m) and maximum velocity (V_m) of H_2O_2 and TMB substrates with previously reported materials.

Catalysts	Substrates	K_m (mM)	V_m (10^{-8} M.s^{-1})	Ref.
HRP	H_2O_2	3.70	8.71	[24]
HRP	TMB	0.43	10.00	[24]
$CuFe_2O_4/Cu_9S_8/PPy$	H_2O_2	23.83	9.82	[47]
$CuFe_2O_4/Cu_9S_8/PPy$	TMB	0.13	6.97	[47]
Co_3O_4 gilly-flower like	H_2O_2	245.00	28.50	[61]
Co_3O_4 gilly-flower like	TMB	0.12	33.20	[61]
MoS_2/PPy	H_2O_2	12.80	15.10	[62]
MoS_2/PPy	TMB	0.41	47.40	[62]
$Bi_2Fe_4O_9$	H_2O_2	0.73	1.56	**This work**
$Bi_2Fe_4O_9$	TMB	0.07	2.17	**This work**

3.5. Colorimetric sensing of dopamine in the presence of $Bi_2Fe_4O_9$ nanozyme

In order to demonstrate the acceptable enzyme-mimetic property of $Bi_2Fe_4O_9$ nanozyme, the optimized H_2O_2/TMB/$Bi_2Fe_4O_9$ system was applied as an indirect platform to sense dopamine. As displayed in **Fig. 5A-B**, the presence of dopamine molecule with an effective inhibiting role, prevents the formation ox-TMB under optimum conditions. A point of fact during the increase of dopamine concentration is the gradual vanishing of the dark-blue color and the decreased number of ox-TMB molecules (**Fig. 5C**). Therefore, the presence of

dopamine effectively prohibited the production of ox-TMB molecules. The color changes of TMB solutions were easily observable by naked eyes and the variation of the UV-vis spectra was recorded at 654 nm. This phenomenon clearly indicated the competition between dopamine and TMB molecules to capture •OH generated in the catalytic decomposition of H_2O_2 molecules. The notable decrease of accessible •OH radicals may be the result of phenolic ring oxidation in dopamine molecules [1, 60]. Generally, dopamine oxidation was accelerated using $Bi_2Fe_4O_9$ nanozyme to produce dopamine o-quinone (DOQ). The defined system outlines a simple colorimetric platform for dopamine sensing that is based on the oxidation of dopamine by utilizing H_2O_2 molecules in presence of $Bi_2Fe_4O_9$ nanozyme and TMB substrate.

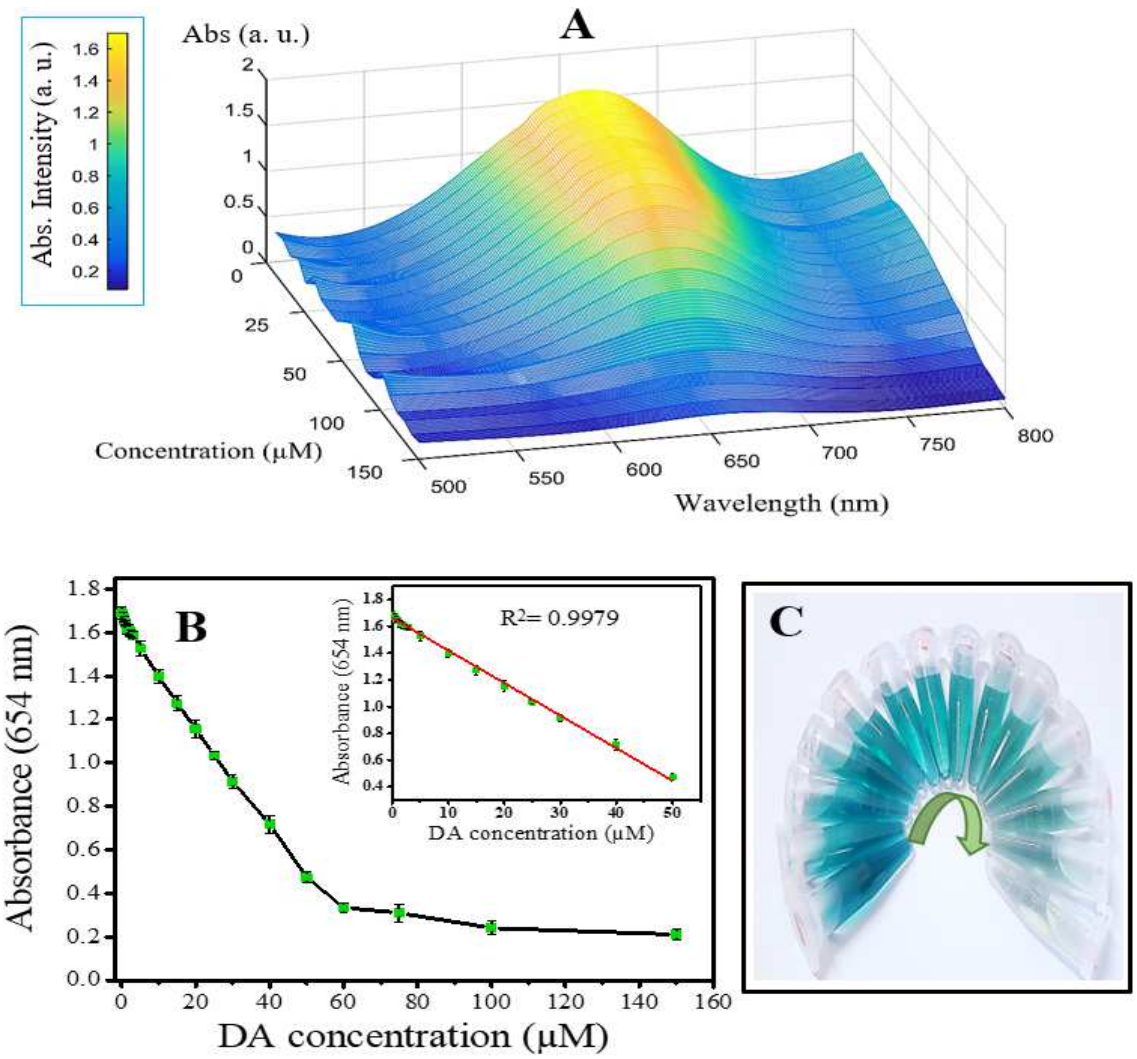

Fig. 5. UV–vis absorption spectra (**A**) and absorbance at 654 nm (**B**) of TMB solutions in presence of $Bi_2Fe_4O_9$ nanozyme and various DA concentrations (0-150 μM). Inset: The linear calibration curve in the lower concentration range of DA (R^2=0.9979). Photographs of the

color-changes during TMB oxidation in presence of different dopamine concentrations (**C**) (from left to right arrow: increasing the concentration of dopamine). Reaction conditions: $Bi_2Fe_4O_9$ NPs (8 µg/mL), TMB (0.3 mM), H_2O_2 (5 mM), acetate buffer (pH 3.5, 0.1 M), T=45 ^oC, and incubation time=25 min. The measurements were performed in triplicates.

An elevation of dopamine concentration from 0 to 150 µM led to a decrease in absorbance intensity of ox-TMB at 654 nm. The color tonality faded from deep-blue to colorless, indicating a decrease in the oxidation rate of TMB oxidation and enhanced formation of dopamine o-quinone molecule (**Fig. 5C**). A good linear range of added dopamine (from 0.15 to 50 µM) to TMB/H_2O_2/$Bi_2Fe_4O_9$ system was obtained by applying the equation A= - 0.024 [dopamine (µM)] +1.663 (R^2=0.9979). In addition, the limit of detection (LOD) was determined to be 51 nM at S/N=3, where S and N represent the signal and noise, respectively.

Table 2 lists the analytical merits of the developed $Bi_2Fe_4O_9$ nanozyme sensor compared to different nanoparticles using various approaches such as electrochemistry [17, 18], electrochemiluminescence [16], fluorescence spectroscopy [13], and colorimetric assays [3, 23]. The value of the LOD of our colorimetric-method by using $Bi_2Fe_4O_9$ nanozyme is lower than previously reported ones. The above results indicate that this designed colorimetric sensor as a simple, facile, and reproducible assay has a high sensitivity to detect dopamine molecules.

Table 2

Method	Sensor	Linear range (μM)	LOD[1] (μM)	Ref.
Electrochemistry	rGO/TiO_2	2-60	0.60	[17]
Electrochemistry	CAuNE	1-100	5.83	[18]
ECL[2]	CdSeTe/ZnS QDs	3.75-450	0.10	[16]
Fluorescence	BSA-CuNCs	0.50-50	0.28	[13]
Colorimetric	$LaCoO_3$	0.50-20	0.19	[3]
Colorimetric	Co_3O_4@NiO	1-1000	1.21	[60]
Colorimetric	CuS/rGO	2-100	0.48	[63]
Colorimetric	Ag NPs	3.20-20	1.20	[64]
Colorimetric	$CuFe_2O_4/Cu_9S_8$/PPy	2-20	1.00	[35]
Colorimetric	h-CuS NCs	2-150	1.67	[65]
Colorimetric	$NiCo_2S_4$-rGO	0.50-100	0.42	[23]
Colorimetric	Bi_2Fe_4O	0.15-50	0.05	**This work**

Comparison of different analytical methods for quantitative analysis of dopamine.

[1] Limit of detection (LOD)

[2] Electrochemiluminescence (ECL)

3.6. Selectivity of $Bi_2Fe_4O_9$ nanozyme-sensor toward dopamine detection

Under the optimized conditions, the selectivity of the proposed $Bi_2Fe_4O_9$ nanozyme was investigated in the presence of different molecules such as alanine (Ala), cysteine (Cys), arginine (Arg), lysine (Lys), glutathione (GSH), uric acid (UA), ascorbic acid (AA), lactose (Lac), glucose (Glu), fructose (Fru), K^+, Na^+, Mg^{2+}, and Ca^{2+}, with the concentration two times higher (100 μM) than the optimized concentration of dopamine. The reduction of UV–vis absorbance intensity in H_2O_2/TMB/$Bi_2Fe_4O_9$/interfering system was compared to control condition (**Fig. 6**). The excellent inhibition role of dopamine in comparison to other molecules (at higher concentration) indicates that ox-TMB product could not easily be generated in the dopamine-containing system.

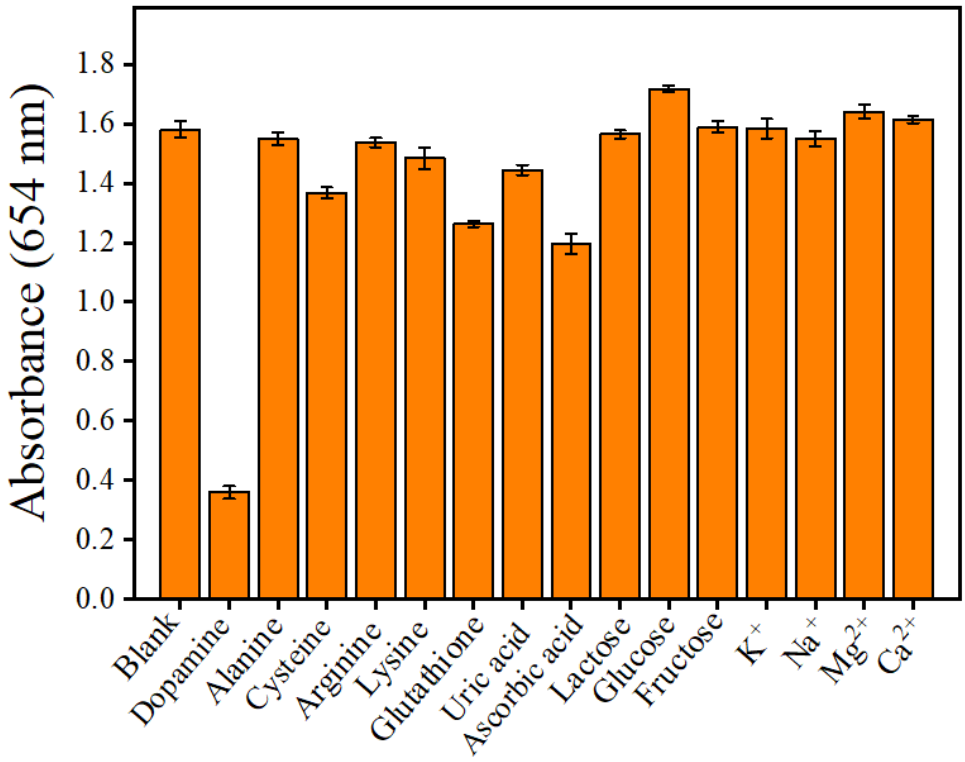

Fig. 6. Absorption at 654 nm of oxTMB in the presence of different interfering molecules at a concentration of 100 µM (2 times higher than the concentration of DA); Reaction conditions: $Bi_2Fe_4O_9$ NPs (8 µg/mL), H_2O_2 (5 mM), TMB (0.3 mM), acetate buffer (0.1 M, pH 3.5), T=45 °C, and incubation time=25 min. The measurements were performed in triplicates.

Dopamine is a strong free radical scavenger and has a potent hydrogen-donating activity. As presented in **Fig. 6**, the excellent inhibition role of dopamine in comparison to the applied interference molecules is obviously reflected from its higher tendency to capture hydroxyl radicals (•OH) in the acidic medium and prohibit the oxidation of TMB molecules. The higher quenching ability of dopamine is related to its specific chemical structure. Dopamine features several H atoms on its aromatic ring responsible for increasing the electron density, mobility, and also the propensity to capture •OH radicals. During the reaction with the reactive oxygen species (ROS) like •OH radical, dopamine is able to produce several derivatives (**Scheme S2 B-D**). As indicated in **Scheme S2**, three initial-hydroxylated products of dopamine are generated during the reaction with •OH radical, namely 2-hydroxydopamine (2-OHDA), 5-hydroxydopamine (5-OHDA), and 6-hydroxydopamine (6-OHDA). All three ring-monohydroxylated dopamine molecules as reactive species could inhibit the oxidation of TMB molecules to oxTMB [1]. Another effective factor of dopamine for inhibiting TMB oxidation is associated with the presence of its ethyl-amine group. The

amine group in the side chain of the dopamine phenolic ring, as a suitable electron-donor group, helps to accelerate electron transfer to enhance the interaction among H atoms on aromatic rings of dopamine with •OH radicals. This result means that dopamine has higher quenching ability of •OH radicals compared to ascorbic acid and uric acid [5, 66]. This oxidation process indicated that the designed colorimetric probe owns a good selectivity and could play an important role in the low detection of dopamine in aqueous media.

3.7. Reproducibility of $Bi_2Fe_4O_9$ nanoparticles

To investigate the nanozyme efficiency, a fresh sample of $Bi_2Fe_4O_9$ NPs (8 µg/mL), TMB (0.3 mM), and H_2O_2 (5 mM) in acetate buffer (pH 3.5, 0.1 M) at 45 °C was slightly shaken for 25 min. The final volume of the solution was 1.5 mL. For the repeated cycle purpose, H_2O_2/TMB/$Bi_2Fe_4O_9$ reaction mixture was centrifuged at 10,000 rpm for 7 min and rinsed with deionized water at 25 °C and then the precipitate was added to H_2O_2/TMB solution under the obtained optimal conditions. The relative activity versus response cycle is depicted in **Fig. S6**. The catalytic stability of $Bi_2Fe_4O_9$ after every catalytic cycle, compared with the original activity, was slightly reduced. After the fourth independent cycle, the primary absorbance intensity of the fresh mixture was decreased from 100% to 93%. The result proved that $Bi_2Fe_4O_9$ NPs exhibit a good enzyme-like catalytic activity, stability, and reproducibility.

3.8. Detection of dopamine in real samples

To evaluate the practical applicability of the proposed $Bi_2Fe_4O_9$ NPs as an efficient enzyme-like catalyst, we examined dopamine determination in fetal bovine serum (FBS), and horse serum (HS) samples. It should be noted that FBS and HS samples before adding the reagents were diluted 1000 times with buffer phosphate saline (PBS 0.1 mM, pH 7.4). Using the optimized conditions ($Bi_2Fe_4O_9$ NPs (8 mg/mL), H_2O_2 (5 mM), TMB (0.3 mM), pH= 3.5, incubation time=25 min, and T=45 °C), different concentrations of dopamine (1, 5, and 10 µM) were spiked into diluted FBS 1 (Sigma-Aldrich), FBS 2 (Fisher Scientific), and HS (Fisher Scientific) solutions.

Moreover, the recovery values and the content of dopamine in real samples were calculated using the obtained calibration curve in **Fig. 5** and the recorded UV–vis absorption spectra at 654 nm for every real sample (FBS 1, FBS 2, and HS). The result of percentage recovery ($[dopamine]_{found}/ [dopamine]_{added} \times 100$) and relative standard deviation (RSD %) are listed in **Table 3**. The relative recoveries of dopamine concentration in FBS (1 and 2) and HS

samples were respectively in the ranges of 96.18–118.12% and 97.61–104.92%. It should be noted that to reduce the stochastic error effect, UV-vis absorbance values were recorded three-times for each experimental condition. The results revealed that this colorimetric method, as a feasible and reliable approach, can be applied to determine dopamine in different real samples.

Table 3

Sensing of DA in fetal bovine serum (FBS 1 and 2), and horse serum (HS) samples (n = 3).

Samples	DA added (μM)	DA founded (μM)	Recovery (%)	RSD (%)
FBS 1	1.00	1.02	101.78	0.39
	5.00	5.35	106.95	0.64
	10.00	9.62	96.18	1.76
FBS 2	1.00	1.16	116.22	1.66
	5.00	5.40	108.02	0.39
	10.00	11.81	118.12	3.81
HS	1.00	0.97	97.61	1.42
	5.00	5.10	102.04	0.80
	10.00	10.49	104.92	3.27

3.9. The investigation of the mimic-enzyme catalytic mechanism to produce hydroxyl radicals (•OH)

To confirm the peroxidase-like mechanism of $Bi_2Fe_4O_9$ NPs, terephthalic acid (TA) molecule was selected as a fluorescence probe. As indicated in **Fig. 7**, TA can react with •OH radicals to yield 2-hydroxyterephthalic acid (HTA) molecule, displaying an intense fluorescence signal [6, 67-69]. The general oxidation reaction of the TA molecule is depicted in the following **Fig. 7A**. All the solutions (**Fig. 7B**) were prepared in acetate buffer (pH 3.5, 0.1 M) and the total value was 1.5 mL. As presented in **Fig. 7B (g, e**, and **c)**, terephthalic acid (TA) did not show an obvious emission peak in the absence of H_2O_2, the presence of H_2O_2 alone, and $Bi_2Fe_4O_9$ NPs alone. It could be clearly seen, in **Fig. 7B (a)**, that the introduction of $Bi_2Fe_4O_9$ nanozyme to TA/H_2O_2 mixture led to the appearance of fluorescence emission with a maximum peak at around 435 nm under optimum experimental conditions, which is a strong indication that TA was converted into HTA molecules. The fluorescence curves indicated that the formation of HTA molecules was highly related to the presence of both

H_2O_2 substrate and $Bi_2Fe_4O_9$ nanozyme in the reaction mixture (H_2O_2/$Bi_2Fe_4O_9$/TA). In the presence of dopamine, the fluorescence intensity of obtained HTA was dramatically decreased, which proved the competitive role of dopamine compared to TA for grasping the hydroxide radicals (**Fig. 7B (b), orange curve**). The fluorescence intensity related to HTA molecules in each of the eight solutions was recorded at 435 nm. The transformation of TA into fluorescent (HTA) molecules was accelerated in the presence of $Bi_2Fe_4O_9$ nanozyme through the decomposition of H_2O_2 molecules into hydroxyl radicals (•OH).

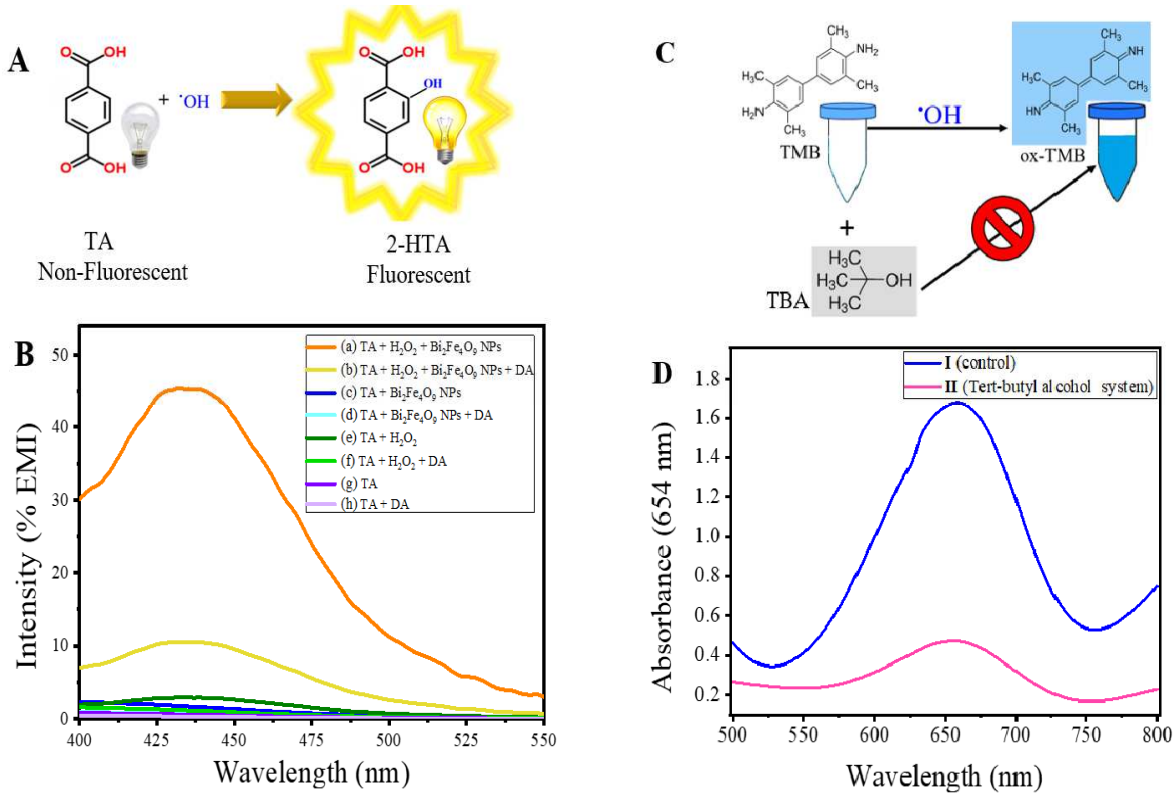

Fig. 7. (A) The possible mechanism of reaction of terephthalic acid (TA) with hydroxyl radicals. (**B**) Fluorescence spectra using TA as a fluorescent probe (λ_{ex}=315 nm), Reaction experimental conditions: (**a**) H_2O_2 (5 mM) + $Bi_2Fe_4O_9$ NPs (8 µg/mL), (**b**) H_2O_2 (5 mM) + $Bi_2Fe_4O_9$ NPs (8 µg/mL) + dopamine (50 µM), (**c**) $Bi_2Fe_4O_9$ NPs (8 µg/mL), (**d**) $Bi_2Fe_4O_9$ NPs (8 µg/mL) + dopamine (50 µM), (**e**) H_2O_2 (5 mM), (f) H_2O_2 (5 mM) + dopamine (50 µM), (**g**) only TA (0.2 mM), and (**h**) TA (0.2 mM) + dopamine (50 µM) in acetate buffer (pH 3.5, 0.1 M) and all solutions were incubated for 25 min at 45 °C. (**C**) The proposed mechanism of effect of *tert*-butyl alcohol (TBA) on the peroxidase-mimic catalytic activity of $Bi_2Fe_4O_9$ NPs. (**D**) UV-vis spectra using TBA as an electron scavenger, Reaction experimental conditions: $Bi_2Fe_4O_9$ NPs (8 µg/mL), TMB (0.3 mM), H_2O_2 (5 mM), acetate buffer (pH 3.5, 0.1 M), TBA (0.5 mM), T=45 ºC, and incubation time=25 min.

In addition, to confirm the role of •OH radicals in the reaction mechanism, *tert*-butanol alcohol (TBA) was used as •OH radical scavenger molecule (rate constant = 6.2×10^8 dm^3 mol^{-1} s^{-1}). The presence of TBA obviously prevented the oxidation of TMB molecules and simultaneously produced ($^{\bullet}(CH_3)_3O$) radicals [7, 70]. As mentioned above, TBA can directly quench reactive oxygen species (ROS) as hydroxyl radicals (**Fig. 7C-D**). The comparison of the UV–vis absorption spectra of the H_2O_2/TMB/$Bi_2Fe_4O_9$ (**Fig. 7D, blue curve**) and H_2O_2/TMB/$Bi_2Fe_4O_9$/TBA (**Fig. 7D, pink curve**) systems illustrated an obvious absorption peak in the UV-vis range whose intensity was significantly decreased in the presence of TBA. These phenomena prove that the hydroxyl radicals play an important role in the oxidation of TMB substrate and the charge transfer between Fe (II) to Fe (III) ions in the Fenton-like cycle of $Bi_2Fe_4O_9$ nanozyme.

4. Conclusion

In summary, dopamine (DA) as a neurotransmitter plays a number of key roles in humans and animals. Therefore, the control and monitoring of the amount of dopamine is necessary to prevent disease conditions. In this work, we report, for the first time, a new colorimetric sensor using $Bi_2Fe_4O_9$ nanoparticles with peroxidase-mimic catalytic activity. The metal-based bimetallic $Bi_2Fe_4O_9$ NPs were prepared by a hydrothermal method that is a facile and low-cost approach. $Bi_2Fe_4O_9$ enzyme mimic features high water-solubility and good stability. On the basis of the outstanding catalytic activity of $Bi_2Fe_4O_9$ in the presence of TMB and H_2O_2, a colorimetric sensing platform was developed and exhibited an accurate, highly sensitive, and selective detection of dopamine at a nanomolar level. This colorimetric probe achieved a detection limit and linear concentration range of 51 nM and 0.15-50 μM for dopamine, respectively. The developed sensor outperforms the already reported nanozymes in literature [3, 35, 63-65]. Under optimized experimental conditions, Michaelis-Menten kinetics analysis of the oxidation state of TMB substrate, in H_2O_2/TMB/$Bi_2Fe_4O_9$ system, achieved V_{max} and K_m values of 2.17×10^{-8} $M.s^{-1}$ and 0.07 mM, respectively. To gain a better understanding of the reaction mechanism, we examined the effect of hydroxyl ($^{\bullet}OH$) radicals as important reactive oxygen species to oxidase dopamine molecules in the H_2O_2/TMB/$Bi_2Fe_4O_9$/DA colorimetric-system using terephthalic acid (TA) and *tert*-butyl alcohol (TBA) probes. This spectroscopic method for evaluation of •OH radicals is a simple, inexpensive, and reliable approach. In addition, the potential application of $Bi_2Fe_4O_9$ as a peroxidase-mimic catalyst to accurately detect dopamine concentration in fetal bovine serum

(FBS) and horse serum (HS) samples was demonstrated. Taken together the results of the present study highlight the potential application of nanostructured bismuth ferrite ($Bi_2Fe_4O_9$) in the diagnosis of dopamine-related diseases. Future work will introduce the investigation of dopamine in real samples by using lateral-flow test strips coupled with smartphones. These studies will open new perspectives for early detection and treatment of different types of drug addiction and neurological related diseases.

CRediT authorship contribution statement

Mehri Razavi: Investigation, Methodology, Validation, Visualization, Formal analysis, Writing-original draft. **Alexandre Barras:** Investigation, Methodology. **Majdid Ifires:** Resources. **Abir Swaidan:** Resource. **Maryam Khoshkam:** Investigation. **Sabine Szunerits:** Investigation. **Mohsen Kompany-Zareh:** Writing-reviewing and editing. **Rabah Boukherroub:** Supervision, Conceptualization, Writing-review & editing, Funding acquisition, Project administration.

Declaration of Competing Interest

The authors declare that they have no known competing financial interests or personal relationships that could have appeared to influence the work reported in this paper.

Acknowledgments

The authors wish to thank the Centre National de la Recherche Scientifique (CNRS), the University of Lille, the region Hauts-de-France, the CPER “Photonics for Society”, and the Institute for Advanced Studies in Basic Sciences (IASBS) in Iran for supporting this study.

References

[1] A. Slivka, G. Cohen, Hydroxyl radical attack on dopamine, J. Biol. Chem. 260 (1985) 15466-15472.

[2] J. Liu, L. Yuan, X. Dong, Recent advances in analytical techniques for the determination of dopamine, Int. J. Chem. Stud. 3 (2015) 39-45.

[3] K. Wang, J. Song, X. Duan, J. Mu, Y. Wang, Perovskite $LaCoO_3$ nanoparticles as enzyme mimetics: their catalytic properties, mechanism and application in dopamine biosensing, New J. Chem. 41 (2017) 8554-8560.

[4] P.A. Rasheed, J.-S. Lee, Recent advances in optical detection of dopamine using nanomaterials, Microchim. Acta 184 (2017) 1239-1266.

[5] G.-C. Yen, C.-L. Hsieh, Antioxidant effects of dopamine and related compounds, Biosci. Biotechnol. Biochem. 61 (1997) 1646-1649.

[6] M.N. Ivanova, E.D. Grayfer, E.E. Plotnikova, L.S. Kibis, G. Darabdhara, P.K. Boruah, M.R. Das, V.E. Fedorov, Pt-decorated boron nitride nanosheets as artificial nanozyme for detection of dopamine, ACS Appl. Mater. Interfaces 11 (2019) 22102-22112.

[7] A. Swaidan, A. Barras, A. Addad, J.-F. Tahon, J. Toufaily, T. Hamieh, S. Szunerits, R. Boukherroub, Colorimetric sensing of dopamine in beef meat using copper sulfide encapsulated within bovine serum albumin functionalized with copper phosphate (CuS-BSA-$Cu_3(PO_4)_2$) nanoparticles, J. Colloid Interface Sci. 582 (2021) 732-740.

[8] S. Rostami, A. Mehdinia, A. Jabbari, Intrinsic peroxidase-like activity of graphene nanoribbons for label-free colorimetric detection of dopamine, Mater. Sci. Eng. C 114 (2020) 111034-111044.

[9] G.E. De Benedetto, D. Fico, A. Pennetta, C. Malitesta, G. Nicolardi, D.D. Lofrumento, F. De Nuccio, V. La Pesa, A rapid and simple method for the determination of 3, 4-dihydroxyphenylacetic acid, norepinephrine, dopamine, and serotonin in mouse brain homogenate by HPLC with fluorimetric detection, J. Pharm. Biomed. Anal. 98 (2014) 266-270.

[10] H. Fang, M.L. Pajski, A.E. Ross, B.J. Venton, Quantitation of dopamine, serotonin and adenosine content in a tissue punch from a brain slice using capillary electrophoresis with fast-scan cyclic voltammetry detection, Anal. Methods 5 (2013) 2704-2711.

[11] Y. Dong, H. Chen, Y. Chen, Y. Hui, X. Chen, Z. Hu, Separation and determination of epinephrine and dopamine in traditional Chinese medicines by micellar electrokinetic capillary chromatography with laser induced fluorescence detection, J. Sep. Sci. 29 (2006) 2049-2055.

[12] S.J. Park, S.H. Lee, H. Yang, C.S. Park, C.-S. Lee, O.S. Kwon, T.H. Park, J. Jang, Human dopamine receptor-conjugated multidimensional conducting polymer nanofiber membrane for dopamine detection, ACS Appl. Mater. Interfaces 8 (2016) 28897-28903.

[13] Z. Miao, W. Hou, M. Liu, Y. Zhang, S. Yao, BSA capped bi-functional fluorescent Cu nanoclusters as pH sensor and selective detection of dopamine, New J. Chem. 42 (2018) 1446-1456.

[14] B. Xu, Y. Su, L. Li, R. Liu, Y. Lv, Thiol-functionalized single-layered MoS_2 nanosheet as a photoluminescence sensing platform via charge transfer for dopamine detection, Sens. Actuators B 246 (2017) 380-388.

[15] W.Z.W. Ismail, G. Liu, K. Zhang, E.M. Goldys, J.M. Dawes, Dopamine sensing and measurement using threshold and spectral measurements in random lasers, Opt. Express 24 (2016) A85-A91.

[16] A.J. Stewart, J. Hendry, L. Dennany, Whole blood electrochemiluminescent detection of dopamine, Anal. Chem. 87 (2015) 11847-11853.

[17] G.T.S. How, A. Pandikumar, H.N. Ming, L.H. Ngee, Highly exposed {001} facets of titanium dioxide modified with reduced graphene oxide for dopamine sensing, Sci. Rep. 4 (2014) 1-8.
[18] D.-S. Kim, E.-S. Kang, S. Baek, S.-S. Choo, Y.-H. Chung, D. Lee, J. Min, T.-H. Kim, Electrochemical detection of dopamine using periodic cylindrical gold nanoelectrode arrays, Sci. Rep. 8 (2018) 1-10.
[19] H. Wei, E. Wang, Nanomaterials with enzyme-like characteristics (nanozymes): next-generation artificial enzymes, Chem. Soc. Rev. 42 (2013) 6060-6093.
[20] Y. Lin, J. Ren, X. Qu, Catalytically active nanomaterials: a promising candidate for artificial enzymes, Acc. Chem. Res. 47 (2014) 1097-1105.
[21] N. Chaibakhsh, Z. Moradi-Shoeili, Enzyme mimetic activities of spinel substituted nanoferrites (MFe_2O_4): A review of synthesis, mechanism and potential applications, Mater. Sci. Eng. C 99 (2019) 1424-1447.
[22] A. Swaidan, A. Addad, J.-F. Tahon, A. Barras, J. Toufaily, T. Hamieh, S. Szunerits, R. Boukherroub, Ultrasmall CuS-BSA-$Cu_3(PO_4)_2$ nanozyme for highly efficient colorimetric sensing of H_2O_2 and glucose in contact lens care solutions and human serum, Anal. Chim. Acta 1109 (2020) 78-89.
[23] Y. Wang, L. Yang, Y. Liu, Q. Zhao, F. Ding, P. Zou, H. Rao, X. Wang, Colorimetric determination of dopamine by exploiting the enhanced oxidase mimicking activity of hierarchical $NiCo_2S_4$-rGO composites, Microchim. Acta 185 (2018) 1-9.
[24] L. Gao, J. Zhuang, L. Nie, J. Zhang, Y. Zhang, N. Gu, T. Wang, J. Feng, D. Yang, S. Perrett, Intrinsic peroxidase-like activity of ferromagnetic nanoparticles, Nat. Nanotechnol. 2 (2007) 577-583.
[25] R. Awasthi, B. Das, Effect of temperature on physical properties of $Bi_2Fe_4O_9$ polycrystalline materials, J. Aust. Ceram. Soc. 56 (2020) 243-250.
[26] Z.-T. Hu, S.K. Lua, X. Yan, T.-T. Lim, Nanostructured hexahedron of bismuth ferrite clusters: delicate synthesis processes and an efficient multiplex catalyst for organic pollutant degradation, RSC Adv. 5 (2015) 86891-86900.
[27] B. Li, C. Lai, G. Zeng, L. Qin, H. Yi, D. Huang, C. Zhou, X. Liu, M. Cheng, P. Xu, Facile hydrothermal synthesis of Z-scheme $Bi_2Fe_4O_9$/Bi_2WO_6 heterojunction photocatalyst with enhanced visible light photocatalytic activity, ACS Appl. Mater. Interfaces 10 (2018) 18824-18836.
[28] A. Poghossian, H. Abovian, P. Avakian, S. Mkrtchian, V. Haroutunian, Bismuth ferrites: New materials for semiconductor gas sensors, Sens. Actuators B 4 (1991) 545-549.
[29] N. Zakharchenko, Catalytic properties of the Fe_2O_3–Bi_2O_3 system in ammonia oxidation to nitrogen oxides, Kinet. Catal. 43 (2002) 95-98.
[30] Z.-T. Hu, J. Liu, X. Yan, W.-D. Oh, T.-T. Lim, Low-temperature synthesis of graphene/ $Bi_2Fe_4O_9$ composite for synergistic adsorption-photocatalytic degradation of hydrophobic pollutant under solar irradiation, Chem. Eng. J. 262 (2015) 1022-1032.
[31] M. Kong, H. Song, F. Li, D. Dai, H. Gao, Facile synthesis of $Bi_2Fe_4O_9$ nanoplate and its application as a novel adsorbent for Cu (II) removal, J. Environ. Chem. Eng. 5 (2017) 69-78.
[32] A. Roy, R. Gupta, A. Garg, Multiferroic memories, Adv. Condens. Matter Phys. 2012 (2012) 1-12.
[33] J. Scott, Multiferroic memories, Nat. Mater. 6 (2007) 256-257.
[34] J.T. Han, Y.H. Huang, X.J. Wu, C.L. Wu, W. Wei, B. Peng, W. Huang, J.B. Goodenough, Tunable synthesis of bismuth ferrites with various morphologies, Adv. Mater. 18 (2006) 2145-2148.
[35] Z. Yang, F. Ma, Y. Zhu, S. Chen, C. Wang, X. Lu, A facile synthesis of $CuFe_2O_4$/Cu_9S_8/PPy ternary nanotubes as peroxidase mimics for the sensitive colorimetric detection of H_2O_2 and dopamine, Dalton Trans. 46 (2017) 11171-11179.

[36] Q. Chen, C. Liang, X. Zhang, Y. Huang, High oxidase-mimic activity of Fe nanoparticles embedded in an N-rich porous carbon and their application for sensing of dopamine, Talanta 182 (2018) 476-483.
[37] X. Wang, M. Zhao, Y. Song, Q. Liu, Y. Zhang, Y. Zhuang, S. Chen, Synthesis of $ZnFe_2O_4$/ZnO heterostructures decorated three-dimensional graphene foam as peroxidase mimetics for colorimetric assay of hydroquinone, Sens. Actuators B 283 (2019) 130-137.
[38] Y. Xing, M. Chen, Y. Zhao, J. Xu, X. Hou, Triple-enzyme mimetic activity of Fe_3O_4@ C@MnO_2 composites derived from metal–organic frameworks and their application to colorimetric biosensing of dopamine, Microchim. Acta 189 (2022) 1-10.
[40] J. Yu, D. Ma, L. Mei, Q. Gao, W. Yin, X. Zhang, L. Yan, Z. Gu, X. Ma, Y. Zhao, Peroxidase-like activity of MoS_2 nanoflakes with different modifications and their application for H_2O_2 and glucose detection, J. Mater. Chem. B 6 (2018) 487-498.
[41] F. Yu, Y. Huang, A.J. Cole, V.C. Yang, The artificial peroxidase activity of magnetic iron oxide nanoparticles and its application to glucose detection, Biomaterials 30 (2009) 4716-4722.
[42] P.D. Liyanage, P. Weerathunge, M. Singh, V. Bansal, R. Ramanathan, L-Cysteine as an Irreversible Inhibitor of the Peroxidase-Mimic Catalytic Activity of 2-Dimensional Ni-Based Nanozymes, Nanomaterials 11 (2021) 1285-1298.
[43] F. Ma, H. Zhao, Optical, Magnetic, Ferroelectric Properties and Photocatalytic Activity of $Bi_2Fe_4O_9$ Nanoparticles through a Hydrothermal Assisted Sol-Gel Method, Russ. J. Phys. Chem. A 93 (2019) 2079-2086.
[44] J. Zhao, T. Liu, Y. Xu, Y. He, W. Chen, Synthesis and characterization of $Bi_2Fe_4O_9$powders, Mater. Chem. Phys. 128 (2011) 388-391.
[45] Z.-T. Hu, S.K. Lua, T.-T. Lim, Cuboid-like $Bi_2Fe_4O_9$/Ag with graphene-wrapping tribrid composite with superior capability for environmental decontamination: nanoscaled material design and visible-light-driven multifunctional catalyst, ACS Sustain. Chem. Eng. 3 (2015) 2726-2736.
[46] Y. Wang, M. Daboczi, C.A. Mesa, S.R. Ratnasingham, J.-S. Kim, J.R. Durrant, S. Dunn, H. Yan, J. Briscoe, $Bi_2Fe_4O_9$ thin films as novel visible-light-active photoanodes for solar water splitting, J. Mater. Chem. A 7 (2019) 9537-9541.
[47] H. Yang, J. Dai, L. Wang, Y. Lin, F. Wang, P. Kang, A novel approach to prepare $Bi_2Fe_4O_9$ flower-like spheres with enhanced photocatalytic performance, Sci. Rep. 7 (2017) 1-11.
[48] M.O. Amin, B. D'Cruz, M. Madkour, E. Al-Hetlani, Magnetic nanocomposite-based SELDI probe for extraction and detection of drugs, amino acids and fatty acids, Microchim. Acta 186 (2019) 1-10.
[49] L. Li, P. Ma, S. Hussain, L. Jia, D. Lin, X. Yin, Y. Lin, Z. Cheng, L. Wang, FeS_2/carbon hybrids on carbon cloth: a highly efficient and stable counter electrode for dye-sensitized solar cells, Sustain. Energy Fuels 3 (2019) 1749-1756.
[50] B. Hu, J.-F. Wang, J. Zhang, Z.-B. Gu, S.-T. Zhang, Synthesis, structures and properties of single phase $BiFeO_3$ and $Bi_2Fe_4O_9$ powders by hydrothermal method, J. Mater. Sci.: Mater. Electron. 26 (2015) 6887-6891.
[51] Y. Du, Z. Cheng, S. Dou, X. Wang, Tunable morphology and magnetic properties of Bi2Fe4O9 nanocrystal synthesized by hydrothermal method, J. Nanosci. Nanotechnol. 11 (2011) 2691-2695.
[52] T.-J. Park, G.C. Papaefthymiou, A.R. Moodenbaugh, Y. Mao, S.S. Wong, Synthesis and characterization of submicron single-crystalline $Bi_2Fe_4O_9$ cubes, J. Mater. Chem. 15 (2005) 2099-2105.
[53] X. Wang, M. Zhang, P. Tian, W. Chin, C. Zhang, A facile approach to pure-phase $Bi_2Fe_4O_9$ nanoparticles sensitive to visible light, Appl. Surf. Sci. 321 (2014) 144-149.

[54] P. Salgado, V. Melin, D. Contreras, Y. Moreno, H.D. Mansilla, Fenton reaction driven by iron ligands, J. Chil. Chem. Soc. 58 (2013) 2096-2101.
[55] C. Von Sonntag, Advanced oxidation processes: mechanistic aspects, Water Sci. Technol. 58 (2008) 1015-1021.
[56] E.S. Henle, Y. Luo, S. Linn, Fe^{2+}, Fe^{3+}, and oxygen react with DNA-derived radicals formed during iron-mediated Fenton reactions, Biochemistry 35 (1996) 12212-12219.
[57] M. Zhao, J. Huang, Y. Zhou, X. Pan, H. He, Z. Ye, X. Pan, Controlled synthesis of spinel $ZnFe_2O_4$ decorated ZnO heterostructures as peroxidase mimetics for enhanced colorimetric biosensing, Chem. Commun. 49 (2013) 7656-7658.
[58] M. Pooladi, I. Sharifi, M. Behzadipour, A review of the structure, magnetic and electrical properties of bismuth ferrite ($Bi_2Fe_4O_9$), Ceram. Int. 46 (2020) 18453-18463.
[59] Y. Liu, C. Wang, N. Cai, S. Long, F. Yu, Negatively charged gold nanoparticles as an intrinsic peroxidase mimic and their applications in the oxidation of dopamine, J. Mater. Sci. 49 (2014) 7143-7150.
[60] Y. Zhu, Z. Yang, M. Chi, M. Li, C. Wang, X. Lu, Synthesis of hierarchical Co_3O_4@ NiO core-shell nanotubes with a synergistic catalytic activity for peroxidase mimicking and colorimetric detection of dopamine, Talanta 181 (2018) 431-439.
[61] J. Yin, H. Cao, Y. Lu, Self-assembly into magnetic Co_3O_4 complex nanostructures as peroxidase, J. Mater. Chem. 22 (2012) 527-534.
[62] J. Lei, X. Lu, G. Nie, Z. Jiang, C. Wang, One-Pot Synthesis of Algae-Like MoS_2/PPy Nanocomposite: A Synergistic Catalyst with Superior Peroxidase-Like Catalytic Activity for H_2O_2 Detection, Part. Part. Syst. Charact. 32 (2015) 886-892.
[63] S. Dutta, C. Ray, S. Mallick, S. Sarkar, R. Sahoo, Y. Negishi, T. Pal, A gel-based approach to design hierarchical CuS decorated reduced graphene oxide nanosheets for enhanced peroxidase-like activity leading to colorimetric detection of dopamine, J. Phys. Chem. C 119 (2015) 23790-23800.
[64] M.R.H. Nezhad, J. Tashkhourian, J. Khodaveisi, M.R. Khoshi, Simultaneous colorimetric determination of dopamine and ascorbic acid based on the surface plasmon resonance band of colloidal silver nanoparticles using artificial neural networks, Anal. Methods 2 (2010) 1263-1269.
[65] J. Zhu, X. Peng, W. Nie, Y. Wang, J. Gao, W. Wen, J.N. Selvaraj, X. Zhang, S. Wang, Hollow copper sulfide nanocubes as multifunctional nanozymes for colorimetric detection of dopamine and electrochemical detection of glucose, Biosens. Bioelectron. 141 (2019) 111450-111466.
[66] H.W. Richter, W.H. Waddell, Mechanism of the oxidation of dopamine by the hydroxyl radical in aqueous solution, J. Am. Chem. Soc. 105 (1983) 5434-5440.
[67] J.C. Barreto, G.S. Smith, N.H. Strobel, P.A. McQuillin, T.A. Miller, Terephthalic acid: a dosimeter for the detection of hydroxyl radicals in vitro, Lif Sci. 56 (1994) PL89-PL96.
[68] Z. Xiang, Y. Wang, P. Ju, D. Zhang, Optical determination of hydrogen peroxide by exploiting the peroxidase-like activity of $AgVO_3$ nanobelts, Microchim. Acta 183 (2016) 457-463.
[69] X. Lai, Y. Han, J. Zhang, J. Zhang, W. Lin, Z. Liu, L. Wang, Peroxidase-Like Platinum Clusters Synthesized by Ganoderma lucidum Polysaccharide for Sensitively Colorimetric Detection of Dopamine, Molecules 26 (2021) 2738-2751.
[70] M. Alam, B. Rao, E. Janata, OH reactions with aliphatic alcohols: evaluation of kinetics by direct optical absorption measurement. A pulse radiolysis study, Radiat. Phys. Chem. 67 (2003) 723-728.